

Tunnel-coupled one-dimensional electron systems with large subband separations

S. F. Fischer,* G. Apetrii, and U. Kunze

Werkstoffe und Nanoelektronik, Ruhr-Universität Bochum, D-44780 Bochum, Germany

D. Schuh and G. Abstreiter

Walter Schottky Institut, Technische Universität München, Am Coulombwall, D-85748 Garching, Germany

(Received 17 May 2006; published 26 September 2006)

One-dimensional (1D) ballistic electron transport is studied through nearly identical stacked 1D quantum conductors separated by a thin tunneling barrier. In contrast to previous works, the 1D electron systems are prepared to exhibit large 1D subband spacings of more than 10 meV. Degeneracies of 1D subbands of equal lateral mode index are lifted and show energy splittings of up to 5.4 meV between symmetric and antisymmetric states. This allows an unprecedented resolution in longitudinal magnetotransport spectroscopy which leads to the observation of an oscillatory mode-dependent variation in the anticrossings of 1D-subband edges of equal lateral mode index.

DOI: [10.1103/PhysRevB.74.115324](https://doi.org/10.1103/PhysRevB.74.115324)

PACS number(s): 73.63.Nm, 73.23.Ad, 72.20.My, 73.21.Hb

I. INTRODUCTION

Electron transport through coupled one-dimensional (1D) quantum conductors is of fundamental interest for the understanding and realization of coherent quantum superposition states in a solid state environment and of potential interest for future quantum electronic devices such as bidirectional couplers,¹⁻³ quantum wave guide inverters,⁴ and quantum wave guide networks.⁵

1D electron systems that show conductance quantization are often referred to as short quantum wires, electron wave guides or quantum point contacts. Usually the 1D confinement can be approximated by a saddlepoint potential⁶ $V(y) = V_0 - \frac{1}{2}m\omega_x^2x^2 + \frac{1}{2}m\omega_y^2y^2$, where x is the direction of free electron movement and y that of the 1D lateral confinement. At the saddlepoint center the harmonic oscillator (HO) potential $V(x=0, y)$ determines the formation of discrete 1D-subband edges at the HO eigenenergies $E_n = (n+1/2)\hbar\omega_y$, where $n = 1, 2, 3, \dots$ is the lateral mode index. 1D-subband separations are then given by $\Delta E = \hbar\omega_y$. The stationary HO eigenstates represent a set of orthogonal wave functions⁷ $\phi_n(y)$.

This work is on mode-coupling⁸ between two identical harmonic quantum mechanical oscillators representing the lateral modes in a top (t) and bottom (b) 1D electron system. A tunnel barrier is situated between the two conductors stacked in a z direction. The tunnel interaction between lateral modes n and m of the top and bottom system, respectively, is governed by a nonzero matrix element^{9,10} $M = \langle \Psi_{nt} | V(z) | \Psi_{mb} \rangle$ with the total wave functions $\Psi_j(x, y, z) = e^{-ik_x x} \phi_j(y) \chi_j(z)$ and $j = nt$ or mb . The eigenstates of different modes ($n \neq m$) are orthogonal⁷ and will turn M to zero for a separable confining potential. For the equal mode index ($n = m$) the formation of symmetric and antisymmetric coupled wave functions is expected and will lead to splitting of the degenerate 1D-subband edges. Our particular interest is to experimentally establish this ideal case and to investigate the influence of a longitudinal magnetic field which couples the y and z component in the electron wave function.

Closely spaced coupled 1D electron systems can be prepared by local depletion of stacked two-dimensional electron

gases (2DEGs) contained in double-quantum-well (DQW) GaAs/AlGaAs heterostructures with AlGaAs or AlAs barriers grown by molecular-beam epitaxy. Thus the tunneling barrier thickness can be controlled on the atomic scale.

Hitherto, vertically stacked coupled 1D systems were defined electrostatically by split-gate structures.¹⁰⁻¹⁴ Repulsion of degenerate 1D subband edges was found as a cause of tunnel coupling.¹⁰⁻¹² However, different findings of mode coupling in longitudinal fields^{10,11} remain to be explained. The systems used in these works had 1D subband separations of only a few meV which limits the resolution, restricts the operation to the mK regime, and renders a single-mode control difficult.

In order to operate in a reliable single-mode control it is of utmost importance to achieve much larger 1D subband separations. Recently, we demonstrated transport (energy) spectroscopy of the two independent 1D subladders and resolved the energy splitting between the mode-coupled subband edges for 1D systems with large subband spacings.¹⁵

Here, we detail the influence of the 1D confinement, applied electric and magnetic fields, and cooling bias on the tunnel coupling for vertically stacked short ballistic 1D electron systems with 1D-subband separations in excess of 10 meV for which an operating temperature 4.2 K is common. A strong lateral 1D confinement is achieved with local barriers formed by etched nanogrooves.^{16,17} In contrast to split-gate structures the groove-defined structures are covered by a single top gate. Tunnel-coupling is distinguished from degenerate decoupled modes by varying both the top gate and back gate voltages. Cooling bias¹⁸ and magnetic fields are applied to identify the 1D modes and influence the mode coupling.

II. EXPERIMENTAL DETAILS

The vertically stacked dual 1D electron systems were prepared from a DQW heterostructure consisting of two equally wide (14.5 nm) GaAs layers forming the quantum wells (QW) separated by a 1 nm thick $\text{Al}_{0.32}\text{Ga}_{0.68}\text{As}$ barrier. The upper bound of the top QW is situated 60 nm below the

heterostructure surface. Electrons are provided by two delta-doped supply layers, each on one side of the DQW. A sheet electron density of $4.3 \times 10^{11} \text{ cm}^{-2}$ and a mobility of $2.4 \times 10^5 \text{ cm}^2 \text{ V}^{-1} \text{ s}^{-1}$ were measured in the dark at 4.2 K for the ungated structure.

Dynamic ploughing with an atomic force microscope (AFM) was used to define nanoscale furrows in a 7 nm-thin resist on the central channel area of a modulation-doped field-effect transistor.¹⁷ The pattern was transferred by subsequent wet-chemical etching with an aqueous citric acid solution. A topography image of etched nanogrooves is shown in the inset of Fig. 2(b). Etching depths in excess of 50 nm guarantee the simultaneous depletion of both 2DEGs of the DQW underneath the etched grooves forming two vertically stacked bottom and top 1D constrictions which each are connected to the bottom and top QW, respectively. The QW reservoirs have common alloyed AuGe/Ni source and drain contacts. An Au top gate covers the constriction, and the back side of the sample serves as a back gate.

Two-terminal differential conductance and transconductance measurements were performed by means of a standard lock-in technique at 4.2 K. The drain excitation voltage was 0.3 mV rms at 433 Hz. Additionally, for transconductance measurements under zero drain bias the top-gate voltage was modulated with a 3 mV rms voltage. Bias spectroscopy is performed by applying a finite dc drain bias voltage and measuring the conductance from which the transconductance is calculated as the derivative with respect to the top gate voltage. Measurements under longitudinal magnetic fields were performed at a sample temperature of 2 K.

III. RESULTS

A. Tunnel-coupled two-dimensional reservoirs

In order to investigate coupling phenomena in the electron transport through nanostructures made from vertically stacked tunnel-coupled 2DEGs it is important to separate any contribution from the tunnel-coupling in the 2D reservoirs. The behavior of the conductance with increasing electron population in the QWs (increasing top gate voltage), the sequence of QW population, and any difference in the electron densities needs to be known in detail. In particular all parameters of the coupling regime (top gate voltage, densities, energy splitting) have to be determined.

First, we discuss the 2D conductance for zero cooling bias. The QW electron densities n_1 and n_2 were determined by Shubnikov-de Haas (SdH) measurements. The conductance characteristics of the DQW heterostructure as shown in Fig. 1(a) depicts a threshold in the top gate voltage V_{tg} which is correlated to the onset of population of a 2D-ground state for one QW as can be seen in Fig. 1(b). At small top gate voltages only one QW serves as a 2D transport channel which leads to a linear increase of the density n_1 and an increase in conductance with raised V_{tg} .

At $V_{\text{tg}} = -0.16 \text{ V}$ the conductance shows a maximum and a second SdH oscillation is resolved for higher V_{tg} , indicating the onset of the population of a second 2D channel with a density n_2 . For further increased top gate voltages a conductance minimum reflects an increased interchannel Cou-

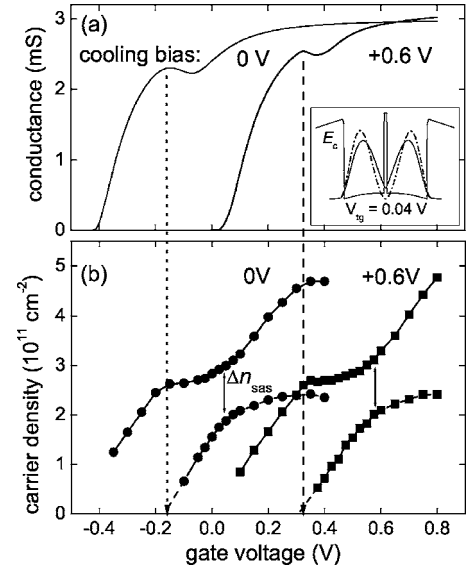


FIG. 1. (a) Conductance of the double QW heterostructure versus top gate voltage after cooling under zero and $V_c = +0.6 \text{ V}$ top-gate voltage from room temperature to $T = 2 \text{ K}$. Inset: calculated conduction band edge E_c of the double QW at the top gate voltage V_{tg} of $+0.04 \text{ V}$ for which the QWs are symmetric and the corresponding squared amplitudes of the wave function for the split symmetric (solid) and antisymmetric (dashed-dotted) eigenstates; no cooling bias. (b) QW electron densities versus top gate voltage extracted from Shubnikov-de Haas measurements at $T = 2 \text{ K}$.

lomb scattering and indicates a difference in the mobility of the two QWs which is associated to the difference in the QW densities.

The secondly populated QW has a poor mobility μ_2 near the occupation onset due to its lower density n_2 . As a consequence, for a certain top gate voltage range the second high-resistance channel [$R_2 = (\mu_2 n_2 e)^{-1}$] is shortened by the first low-resistance channel (R_1).¹⁹

For higher V_{tg} n_1 remains constant while the population of the second channel n_2 increases linearly. At $V_{\text{tg}} \sim +0.04 \text{ V}$ the conduction band edge of the double QW structure is symmetric with respect to the barrier, see the inset of Fig. 1(a), i.e., in balance. More details about the simulated bandstructure and calculated electron densities are given in Ref. 16. Equal densities would occur in the QWs for the decoupled case. However, n_1 and n_2 maintain a minimum separation Δn_{min} at the balance as marked by a double-sided arrow in Fig. 1. These correspond to the split symmetric (n_{sym}) and antisymmetric (n_{asym}) states which are equally extended across both QWs and arise from tunnel coupling. Therefore, the split eigenstates have different mobilities but the occupation of both is equal in the two QWs. The conductance does not show a minimum at the balance point which indicates that the QW mobilities are roughly equal. Samples with different mobilities exhibit maximum resistance when the QWs are balanced due to the delocalization of the electron wave function which causes an increased scattering in the lower-mobility well.²⁰

The coupling strength is characterized by the splitting of the subband edges ΔE_{sas} for symmetric and antisymmetric

states and can be estimated from $\Delta n_{\min} = \Delta n_{\text{sas}}$ by $\Delta E_{\text{sas}} = \frac{\pi \hbar^2}{m^*} \Delta n_{\text{sas}}$. For zero cooling bias $\Delta n_{\text{sas}} \sim 1.1 \times 10^{11} \text{ cm}^{-2}$ is observed at top gate voltage of +0.04 V and the anticrossing energy gap amounts to 3.9 meV.

Further increase of V_{tg} destroys the equilibrium and leads to electron localization in the individual QWs. The population of the second 2D channel increases linearly while that of the first maintains a constant electron density. When the system is out of balance the resistance of the two QWs connected in parallel approaches that of the higher-mobility well.¹⁹

Cooling the sample from room temperature to 4.2 K with an applied positive top gate voltage V_c reduces the effective doping.¹⁸ This technique we apply below to weaken the 1D confining potential of a particular etched 1D constriction. The effect on the 2DEGs is that the threshold voltages for both QW populations increase but the general behavior remains the same as shown in Fig. 1 for the case of cooling under $V_c = +0.6$ V. At $V_{\text{tg}} = +0.31$ V the population of the second 2D channel sets in and at +0.57 V Δn_{sas} amounts to $\sim 1.1 \times 10^{11} \text{ cm}^{-2}$. Therefore, we find no change in the symmetric-antisymmetric energy splitting due to cooling under top gate bias up to $V_c = +0.6$ V.

The evolution of the densities with the gate voltage indicates that the bottom QW which has a larger distance to the top gate is populated first, hence $n_b = n_1$. The other case, namely population of the top QW first, would lead to screening of the gate electric field by the formed electron sheet and thus prevent the filling of the bottom QW. This screening effect manifests itself after the onset of $n_t = n_2$ in the top gate-voltage-independent density of the bottom QW $n_b = n_1$.

Finally, it is noteworthy that tunnel coupling between the QW modes occurs at lower top gate voltages than between 1D modes as shown below. Therefore, transport phenomena arising from 2D and 1D tunnel coupling are clearly distinguishable.

B. Decoupled one-dimensional electron systems

Whether or not a double-layer 1D electron system separated by a tunneling barrier shows coupling phenomena depends strongly on how the 1D confinement acts on electrons of each QW layer. Here, we investigate first the case of decoupled 1D quantum conductors for which electron interaction through the tunnel barrier does not lead to the formation of mode-coupled symmetric and antisymmetric states and, hence, degenerate energy levels do not split up. For equal lateral width of both 1D conductors such is expected for all levels with a different lateral mode index.¹⁰

Typical characteristics of conductance quantization for a decoupled double 1D quantum conductor are shown in Fig. 2(a). In all cases the conductance threshold is at a gate voltage for which electrons in the 2D reservoirs are decoupled and the density of the top QW is about twice that of the bottom QW. As for a single layer 1D electron system, a decrease in the constriction width w leads to an increase in the top gate threshold due to a stronger lateral confinement.

For all three examples in Fig. 2(a) the first conductance plateau in units of $2e^2/h$ is as broad and clearly defined as

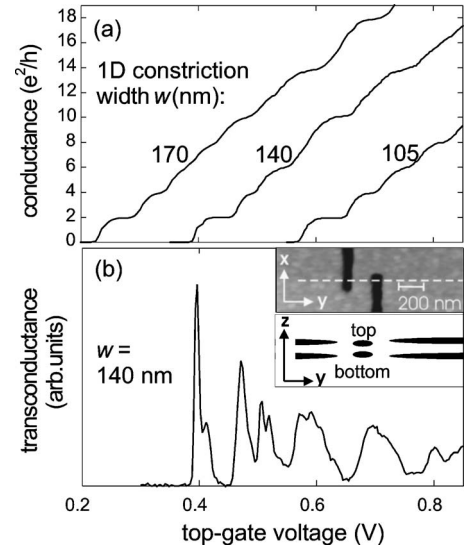


FIG. 2. (a) Quantized conductance measured at $T=4.2$ K of three decoupled double layer 1D electron systems made of 1D constrictions with different widths. The nanogrooves forming the local barriers have an etch depth of 50–55 nm. The conductance was corrected for series resistances ranging from 800 to 1300 ohm. (b) Measured transconductance of the 1D constriction with 140 nm geometric width. The inset depicts the constriction geometry. Top inset: Atomic-force microscopy image of the topography of the 1D constriction before deposition of the Au top gate. Black represents the nanogrooves of 55 nm etch depth in a distance of 140 nm forming the 1D constriction. Bottom inset: Schematic cross-sectional view of the 1D constriction in the top inset along the dashed line. Depletion of electrons in the heterostructure by the nanogrooves and formation of a double 1D electron system in between is indicated by black and white regions, respectively.

for comparable samples with a single 1D electron system indicating that the lowest 1D subband of only *one* subladder is populated.¹⁷ Successive conductance steps become less well defined or are missing after occupation of the second 1D subband system. Thus the measured conductance represents a superposition of the two contributions from the 1D quantum conductors with different threshold voltages.

The transconductance, as shown exemplarily in Fig. 2(b), has maxima at the onset of each conductance step signaling the ongoing occupation of a 1D subband with increasing top gate voltage. Variation of the back gate voltage allows one to shift the 1D subladders relative to each other in a moderate manner. This is visible by plotting the transconductance maxima in gray scale versus top gate and back gate voltages. Fig. 3 clearly shows a different variation for the two 1D subladders.

Two sets of transconductance maxima exist, one of which shifts to lower top gate voltages for increasing back gate voltage while the other appears nearly back-gate independent. Therefore, we identify electrons populating the 1D subladder at lower top gate voltage as stemming from the bottom QW reservoir which can be influenced by the back gate. The 1D electron system arising from the top QW is populated at higher top gate voltages and shows only little response to back gate voltage due to screening by the bottom QW.

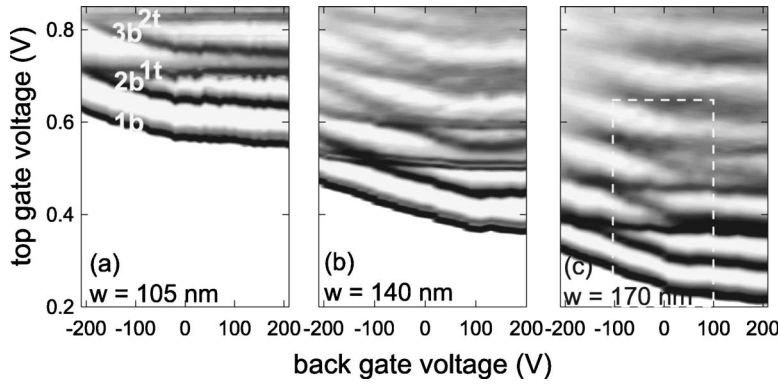


FIG. 3. Gray-scale plots of the measured transconductance versus top gate and back gate voltages for three decoupled double-layer 1D electron systems with different geometric constriction widths [see also Fig. 2(a)]. All measurements were taken at $T=4.2$ K by increasing the back gate from negative to positive voltages after each top gate sweep. The transconductance maxima are plotted in black.

In Fig. 3(a) the transconductance maxima are exemplarily labeled with the corresponding lateral mode index n as 1t, 2t, 3t,... for the subladder of the top QW and 1b, 2b, 3b,... for that of the bottom QW. Level coincidences are observed for levels of different mode index of the two subladders. This is clearly visible for the lower mode indices at lower top gate voltages where the transconductance maxima are strong. At higher mode indices the transconductance maxima decrease which reduces the resolution.

In the systems investigated we find a small reproducible hysteresis effect for forward and backward back gate sweeps. For sweeps from negative to positive back gate voltages the slope decreases which does not occur for sweeps from positive to negative back gate voltages as shown in Fig. 4(a) which shows a section of Fig. 3(c) (sweep from negative to positive back gate voltages). We assume that this behavior

originates from recharging processes in the backside doping layer arising from weak residual parallel conduction. However, no deviation of the level coincidences arise from this hysteretic behavior.

In general, a decreasing lateral 1D constriction width w leads to an increase in the 1D subband separations as for single layer^{17,18} and spatially coincident²¹ 1D electron systems. However, for the etching depth of about 50–55 nm we find that the confining potentials of top and bottom 1D electron systems are nearly equal and that the energetic offset between both 1D subsystems remains the same irrespective of the constriction width. In dual 1D electron systems the subband spacings of each system can be extracted directly from bias spectroscopy.¹⁵ As is shown in Fig. 4(b) we find nearly equal subband spacings of the first two lateral modes which prove similarity between the lateral confining potential for bottom and top 1D systems.

Additional variation of the confining potential can be introduced by cooling the samples under top gate bias.¹⁸ Almost no effect is seen for cooling bias below the threshold voltage of the 1D conductance. Shifts in threshold voltages are observed for higher cooling biases, however, only towards an increase between the threshold voltages of both 1D systems as shown in Fig. 5. Therefore, a situation of degenerate levels with the same mode index cannot be invoked by application of positive cooling biases. As shown below, a tunnel-coupled 1D electron system reacts more sensitively and can turn toward a decoupled system after application of cooling bias.

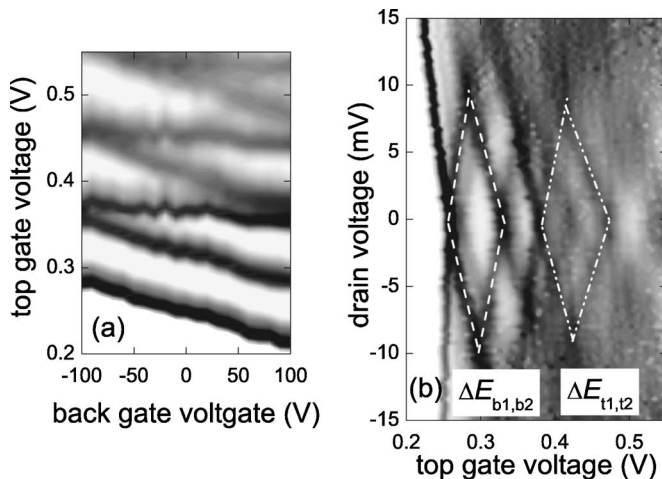


FIG. 4. (a) Gray-scale plot of the measured transconductance versus top gate and back gate voltages for the decoupled double-layer 1D electron systems with a geometric constriction widths of 170 nm. The measurement was taken at $T=4.2$ K by decreasing the back gate from positive to negative voltages after each top gate sweep. Hence, the back gate was swept in reverse compared to the measurement in Fig. 3(c) (for the region indicated by the dotted lines). (b) Gray-scale plot of the transconductance maxima versus top gate and dc drain bias voltage of the decoupled double-layer 1D electron systems with a geometric constriction width of 170 nm. The first 1D-subband spacings for the bottom and top 1D electron system can be read from half the extension of the rhombic pattern as depicted by the dashed and dotted white lines.

C. Coupled one-dimensional electron system

Here, we demonstrate the case of coupling for a 130-nm wide 1D constriction for which the nanogrooves were etched 60–65 nm deep. The conductance characteristic in the case of no cooling bias, see Fig. 6(a), indicates split energy levels as the first conductance plateau is not as pronounced as for the decoupled 1D systems. Furthermore, all subsequent conductance steps are of equal shape and nearly equidistant on the top gate scale. There exist no ill-defined or missing steps as characteristic for added conductances of two independent 1D systems.

The corresponding gray-scale plot of the transconductance maxima versus top gate and back gate voltage clearly gives evidence of level anticrossings, as depicted in Fig. 6(b). Most remarkable when compared to corresponding

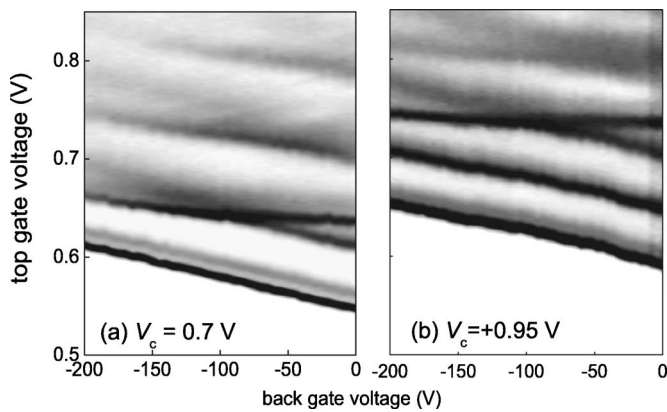


FIG. 5. Gray-scale plots of the measured transconductance versus top gate and back gate voltages for the decoupled double-layer 1D electron systems with a geometric constriction widths of 140 nm after cooling the sample with applied positive top gate voltages. For zero cooling bias see Fig. 3(b). All measurements were taken at $T=4.2$ K by increasing the back gate from negative to positive voltages after each top gate sweep. The transconductance maxima are plotted in black.

plots of decoupled systems; none of the levels appears independent of the back gate. Instead, all transconductance maxima show concave or convex behavior with increasing back gate voltage. However, the plot of a decoupled system can be constructed as indicated by the dashed lines and the level indices marked at back gate voltages ± 200 V. In the decoupled case all back gate independent levels of the top system would cross the bottom levels of equal lateral mode index at about zero back gate voltage. Instead, mode tunnel coupling leads to the observed anticrossings between the levels of (1t,1b), (2t,2b), and (3t,3b).

Direct high-resolution bias spectroscopy of the anticrossings at zero back gate voltage¹⁵ reveals energy level split-

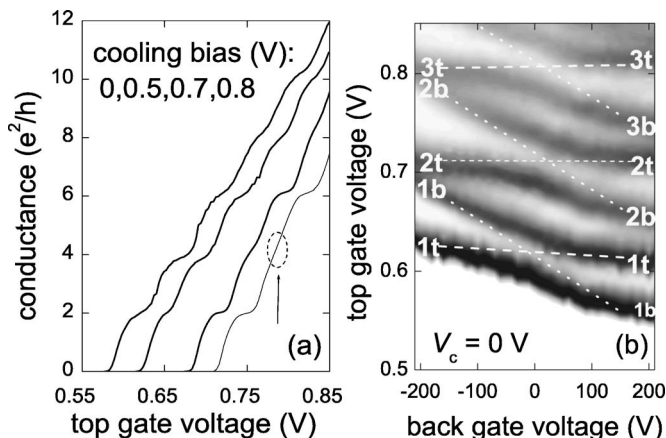


FIG. 6. Transport measurements on a tunnel-coupled 1D bilayer electron system by a 130-nm wide 1D constriction of 60–65-nm deeply etched nanogrooves at 4.2 K. (a) Quantized conductance after cooling the sample under different top gate cooling bias voltages. Corrected for series resistances ranging from 1000 to 1200 ohm. (b) Gray-scale plots of the transconductance maxima versus top gate and back gate voltage. Level anticrossings occur around zero back gate voltage.

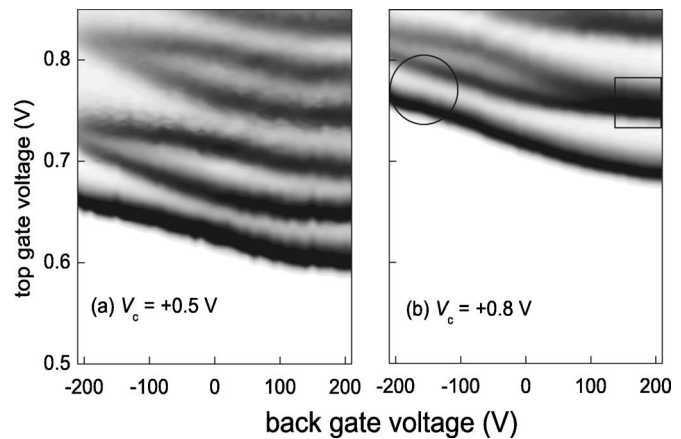


FIG. 7. Gray-scale plots of the transconductance maxima versus top gate and back gate voltage at 4.2 K after cooling the sample under a top gate bias of (a) +0.5 V and (b) +0.8 V for a tunnel-coupled 1D bilayer electron system by a 130-nm wide 1D constriction of 60–65 nm deeply etched nanogrooves.

tings of 5.4, 3.9, and 2.9 meV for the lateral modes indexed 1, 2, and 3, respectively. Correspondingly, tuning the back gate voltage to -210 and 210 V enables the determination of the subband spacings between the first and second 1D subband of the top and bottom 1D electron system and lead to 12.3 and 10.8 meV, respectively.

The verification of mode coupling requires the ability to tune the system from coupling into the decoupled regime. Therefore a minimal relative energetic shift between the two subladders has to be enabled in the order of one subband spacing, here more than 10 meV. Below, we show that this is possible by the application of a cooling bias and magnetic fields.

The mode-coupled system sensitively reacts upon cooling under a positive top gate bias. Cooling the sample under a bias below the threshold voltage $V_t(V_c=0, V_{bg}=0)$ leads to a significant shift in threshold voltage, as shown in the conductance characteristics of Fig. 6(a). For $V_c > V_t(V_c=0, V_{bg}=0)$, see Fig. 6(a), the second plateau vanishes. The missing plateau at $4e^2/h$ after a cooling bias of +0.8 V indicates a level degeneracy for the different lateral modes 1t and 2b.

This finding is supported by the gray-scale plots of the transconductance versus top gate and back gate voltage after cooling under a top gate bias. For $V_c = +0.5$ V $< V_t(V_c=0, V_{bg}=0)$ the anticrossings persist around zero back gate voltage, see Fig. 7(a). However, cooling under $V_c = +0.8$ V changes the pattern significantly. The anticrossings shift toward a negative back gate voltage of -150 V [encircled in Fig. 7(b)]. Furthermore, at a positive back gate voltage of $+200$ V the levels 1t and 2b coincide as marked by a square in Fig. 7(b). Therefore, as in the case of the decoupled system the application of a higher cooling bias can lead to a relative shift of the onset of the two 1D subladders. This allows one to decouple mode-coupled systems.

Mode coupling manifests itself in a peculiar manner when a longitudinal applied magnetic field B_l is applied. In Fig. 8 the evolution of the transconductance maxima (plotted in dark) is shown for the case of no cooling bias. The three figure parts combine the following cases: variation of the

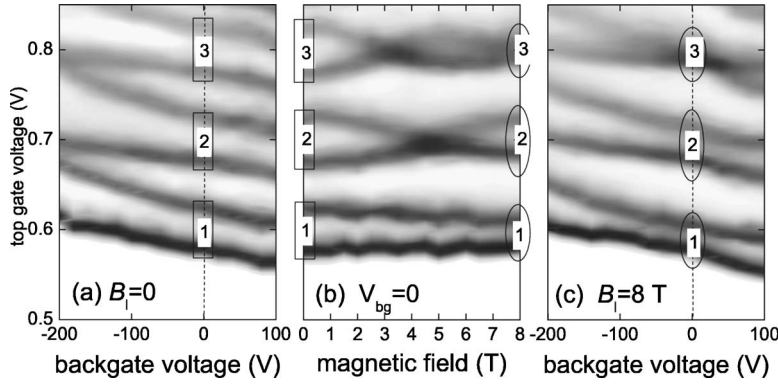


FIG. 8. Gray-scale plots of the transconductance maxima versus top gate and (a) back gate voltage $V_{bg}=0$ at 0 T, (b) an increasing longitudinal applied field ($V_{bg}=0$) and (c) V_{bg} at 8 T for a tunnel-coupled 1D bilayer electron system by a 130-nm wide 1D constriction of 60–65 nm deeply etched nanogrooves. All measurements were taken at 2 K, no cooling bias.

back gate voltage V_{bg} for (a) $B_l=0$, and (c) $B_l=8$ T, and a variation of the magnetic field from 0 to 8 T for (b) $V_{bg}=0$. Evidence is given for an oscillatory variation of the energy splittings with increasing magnetic field.

In Figs. 8(a)–8(c) the identical regions of interest that can be compared between the different measurements at zero back voltage are marked by square and elliptic symbols and labeled with the corresponding lateral mode indices $n=1, 2$, and 3. At zero magnetic field all degenerate levels of identical mode index undergo an anticrossing [Fig. 8(a)] as described above. Increasing the magnetic field [Fig. 8(b)] leads to a decrease between all level splittings of which higher modes are affected stronger. The anticrossing of modes 2t–2b turn into a crossing at 5 T and it reappears up to 8 T. Levels 3t and 3b become degenerate at about 3.2 T then split up for increasing fields and become degenerate again at about 8 T. Figure 8(c) proves this development by the level spectroscopy at 8 T. Compared to the plot of 0 T [Fig. 8(a)] we find at zero back gate voltage: first, the level splitting between 1t–1b is decreased, second, the transconductance maxima of levels 2t and 2b depict an anticrossing and, third, levels 3t and 3b have become degenerate and cross.

IV. DISCUSSION

Compared to previous vertically stacked tunnel-coupled 1D electron systems which were electrostatically defined by

split gates^{10–13} we have fabricated etched 1D constrictions providing much larger 1D-subband separations, as is summarized in Table I. We demonstrated that decoupled and mode-coupled 1D systems can be identified with high resolution at liquid-helium temperature. The splitting energy for mode coupling between the first 1D subbands is twice as high (5.4 meV) as the maximum value reported from split-gate structures¹⁰ (2.6 meV). It represents the case of moderate coupling strength as it is about half of the 1D subband spacings (>10 meV) of the involved individual electron systems.

The case of strong coupling between modes of equal index is known from two works: Thomas *et al.*¹⁰ reported energy splittings of 2.6 meV for the first 1D subbands decreasing to 1.6 meV for the fourth subbands for 1D subband separations of less than 2 meV at 60 mK. Friedland *et al.*¹¹ estimate energy splittings of 0.4 meV for the third 1D subbands and 0.45 meV for the fourth, which increase with an increasing 1D-subband index in contradiction to Ref. 10 and this work. 1D subband spacings were estimated as 0.4 meV at 340 mK.

Reported changes of the anticrossings with longitudinal magnetic field differ in detail. Under in-plane magnetic fields larger than $B=7$ T the anticrossings disappear being replaced by level crossings.¹⁰ This is taken to prove the decoupling of the two QWs due to the relative shift of the Fermi circles such that they no longer overlap. Smaller in-plane magnetic fields parallel to the current are found to cause strong mixing of the 1D wave functions leading to complicated crossings

TABLE I. Parameters and results of vertically stacked bilayer 1D electron systems made from double quantum well GaAs/AlGaAs heterostructures separated by a AlGaAs tunneling barrier for which 1D-mode coupling has been observed. Parameters are the single quantum well width w_{QW} , barrier thickness t , 2D electron density n_{2D} , and 2D electron mobility μ_{2D} . Measured results are given for the 2D anticrossing energy gap $\Delta E_{2D,sas}$, the 1D subband spacings $\Delta E_{n,n+1}$, and the energy splittings for tunnel-coupled 1D modes $\Delta E_{1t-1b,sas}$. n.s. denotes “not specified.” T denotes the measuring temperature.

	Ref. 12	Ref. 10	Ref. 13	Ref. 11	This work
w_{QW} (nm)	20	15	15	20	14.5
t (nm)	3.1	3.5	2.5	1.1	1
μ_{2D} (10^6 cm ² /Vs)	3.0	1	1.45	0.58	0.24
$\Delta E_{2D,sas}$ (meV)	0.9	1	1.4	1.7	3.9
$\Delta E_{n,n+1}$ (meV)	0.4	n.s.	<2	n.s.	>10
$\Delta E_{1t-1b,sas}$ (meV)	0.4–0.45	n.s.	2.6	n.s.	2.9–5.4
T (K)	0.34	0.5	0.06	0.3	4.2

and anticrossings at 2 T in one work¹⁰ while in another¹¹ a decrease of the 1D-anticrossing energy splittings is found when compared to $B=0$ and anticrossings of states with different subband index, with an anticrossing pattern different from that in Ref. 10. A mode-dependent variation of anticrossings and the strong evidence for their oscillatory variation with increasing longitudinal magnetic field as shown in Fig. 8 thus presents a novel observation.

In a simple semiclassical picture, the variations in the anticrossings as shown in Fig. 8 can qualitatively be understood as follows. A magnetic field B applied along the quantum channel in the x direction can be expressed in terms of the vector potential A as $B_x = \partial A_z / \partial y - \partial A_y / \partial z$ with $A_y = -1/2zB$ and $A_z = -1/2yB$. Due to the canonical momentum $\mathbf{p} - e\mathbf{A} = \hbar\mathbf{k}$, the electron gains wave vector components as $\Delta k_y = -e/\hbar(\Delta z/2)B$ and $\Delta k_z = e/\hbar(\Delta y_n/2)B$ when moving along distances Δy or Δz , respectively, in the magnetic field. Here, Δz is the extension of the electron wave function in the case of coupled quantum wells and approximately the same (~ 15 nm) for all lateral modes but Δy_n is mode dependent. It relates to the lateral extension of the electron's wave function $\Delta y_n = \sqrt{\langle \phi^*(y)|y|\phi(y) \rangle} = \sqrt{(n-1/2)\hbar/(m\omega_y)}$ within the harmonic oscillator potential in the saddlepoint of the constriction and yields for example about 7 nm ($n=1$) to 17 nm ($n=3$) for a 1D-subband spacing $\Delta E_{n,n+1}$ of 10 meV. The oscillatory variation of the anticrossings with increasing magnetic field and the appearance of level crossings suggests the influence of a magnetic field induced phase change in the electron wave function on mode coupling. Semiclassically, the electron can perform an orbital motion along the spatial extensions of Δz and Δy_n while crossing the tunnel-coupled constriction. The magnetic change in phase gathered by the

electron amounts to $(e/\hbar)\int \mathbf{A} \cdot d\mathbf{s}$ along the trajectory s . For a closed path the magnetic flux Φ enclosed by the area S will lead to the phase change $(e/\hbar)\oint \mathbf{B} \cdot d\mathbf{S} = 2\pi\Phi/\Phi_0$, where $\Phi_0 = h/e$ is the magnetic flux quantum. A phase change of $q\pi$ with $q=1,3,5,\dots$ in the time the electron passes the constriction may lead to a loss of the phase coherence condition for superposition states involved in mode coupling. However, while our estimates confirm that such oscillatory phase changes are invoked by the applied magnetic field a rigorous semiclassical treatment similar to the description of a two-dimensional electron in a strong magnetic field and an external potential²² will be required for a full understanding.

V. CONCLUSION

Tunnel-coupled one-dimensional electron systems with large subband spacings beyond 10 meV allow single mode control at liquid helium temperature and have a high potential as building blocks for fundamental investigations on coherence phenomena of engineered matter waves in a solid state environment. We investigated the case of nearly identical one-dimensional confining potentials for which the lateral modes can be approximated by the harmonic oscillator eigenstates. Indications for an oscillatory variation of anticrossings in longitudinal magnetic fields are observed.

ACKNOWLEDGMENTS

G.A. gratefully acknowledges the financial support of the Deutsche Forschungsgemeinschaft via Graduiertenkolleg 384 and from the Isolde Dietrich Stiftung. Part of this work was supported by the Bundesministerium für Bildung und Forschung under Grant No. 01BM920.

*Electronic address: Saskia.Fischer@rub.de

- ¹N. Tsukuda, A. D. Wieck, and K. Ploog, *Appl. Phys. Lett.* **56**, 2527 (1990).
- ²C. C. Eugster, J. A. del Alamo, M. J. Rooks, and M. R. Melloch, *Appl. Phys. Lett.* **64**, 3157 (1994).
- ³J. Harris, R. Akis, and D. K. Ferry, *Appl. Phys. Lett.* **79**, 2214 (2001).
- ⁴M. J. Gilbert, R. Akis, and D. K. Ferry, *Appl. Phys. Lett.* **81**, 4284 (2002).
- ⁵A. Bertoni, P. Bordone, R. Brunetti, C. Jacoboni, and S. Reggiani, *Phys. Rev. Lett.* **84**, 5912 (2001).
- ⁶M. Büttiker, *Phys. Rev. B* **41**, 7906 (1990).
- ⁷ $\phi_n(y) = (2^n n! \sqrt{\pi} y_0)^{-1/2} \exp[-\frac{1}{2}(\frac{y}{y_0})^2] H_n(\frac{y}{y_0})$ with $y_0 = \sqrt{\frac{\hbar}{m\omega_y}}$, m is the electron mass and the Hermite polynomials are given by $H(y) = (-1)^n \exp(y^2) \frac{d^n}{dy^n} \exp(-y^2)$. Orthogonality: $\int_{-\infty}^{\infty} \phi_n(y) \phi_m^*(y) dy = \delta_{nm}$.
- ⁸Treatments of mode coupling in: E. Merzbacher, *Quantum Mechanics*, 2nd edition (Wiley, New York, 1970), pp. 428–429 or C. Cohen-Tannoudji, B. Diu, F. Lalo e, *Quantum Mechanics* (John Wiley & Sons, New York, 2005) (Vol. 1), p. 406.
- ⁹N. Mori, P. H. Beton, J. Wang, and L. Eaves, *Phys. Rev. B* **51**, 1735 (1995).
- ¹⁰K. J. Thomas, J. T. Nicholls, M. Y. Simmons, W. R. Tribe, A. G. Davies, and M. Pepper, *Phys. Rev. B* **59**, 12252 (1999).
- ¹¹K. J. Friedland, T. Saki, Y. Hirayama, and K. H. Ploog, *Physica E*

(Amsterdam) **11**, 144 (2001).

- ¹²I. M. Castleton, A. G. Davies, A. R. Hamilton, J. E. F. Frost, M. Y. Simmons, D. A. Ritchie, and M. Pepper, *Physica B* **249–245**, 157 (1998).
- ¹³M. A. Blount, J. S. Moon, J. A. Simmons, S. K. Lyo, J. R. Wendt, and J. L. Reno, *Physica E (Amsterdam)* **6**, 689 (2000).
- ¹⁴S. Roddaro, V. Piazza, F. Beltram, W. Wegscheider, C.-T. Liang, and M. Pepper, *J. Appl. Phys.* **92**, 5304 (2002).
- ¹⁵S. F. Fischer, G. Apetrii, S. Skaberna, U. Kunze, D. Schuh, and G. Abstreiter, *Nat. Phys.* **2**, 91 (2006).
- ¹⁶G. Apetrii, S. F. Fischer, U. Kunze, D. Schuh, and G. Abstreiter, *Physica E (Amsterdam)* **34**, 526 (2006).
- ¹⁷G. Apetrii, S. F. Fischer, U. Kunze, D. Reuter, and A. D. Wieck, *Semicond. Sci. Technol.* **17**, 735 (2002).
- ¹⁸S. F. Fischer, G. Apetrii, S. Skaberna, U. Kunze, D. Reuter, and A. D. Wieck, *Appl. Phys. Lett.* **81**, 2779 (2002).
- ¹⁹A. Palevski, F. Beltram, F. Capasso, L. Pfeiffer, and K. W. West, *Phys. Rev. Lett.* **65**, 1929 (1990).
- ²⁰A. Kurobe, I. M. Castleton, E. H. Linfield, M. P. Grimshaw, K. M. Brown, D. A. Ritchie, M. Pepper, and G. A. C. Jones, *Phys. Rev. B* **50**, 8024 (1994).
- ²¹S. F. Fischer, G. Apetrii, U. Kunze, D. Schuh, and G. Abstreiter, *Phys. Rev. B* **71**, 195330 (2005).
- ²²H. A. Fertig, *Phys. Rev. B* **38**, 996 (1988).